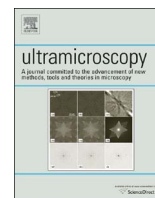




Contents lists available at ScienceDirect

Ultramicroscopy

journal homepage: www.elsevier.com/locate/ultramic

New instrumentation and cutting edge research

A. Howie

Dept. of Physics, University of Cambridge, J.J. Thomson Avenue, Cambridge CB3 0HE, UK

ARTICLE INFO

Keywords:

Projection imaging
Near-field excitation
Phonon imaging

ABSTRACT

Stimulated by Ondrej Krivanek's contributions, the complex interaction between research and innovations in the instrumentation for electron microscopy is discussed. Specific attention is given to aberration correction and to spectroscopy in both the valence region and at the energies of localised phonons or bond vibrations. Current thinking about projection imaging and dielectric excitation theory may be challenged. More significantly in the new fields of investigation opened up to them, electron microscopists will need to build closer relations, particularly with the photonics and scanning tunnelling microscopy communities. Further improvements in instrumentation could usefully be directed towards imaging and spectroscopy at higher scattering angles as well as the incorporation of other facilities such as photon stimulation and secondary electron imaging.

1. Introduction

That overused slogan for science commentaries – “the cutting edge of research” is a concept that more properly springs to mind when discussing the consequences of Ondrej Krivanek's signal contributions to electron microscope instrumentation e.g. [1–3]. Even here however it lacks the clear precision that Occam's razor has long enjoyed in the field of logic. The idea of a sharp linear boundary between the known and the unknown seems indeed far from common experience. More realistically the boundary may be seen in some cases as having a serrated or even a fractal structure. In many cases where the topic is investigated through different techniques by communities in poor communication with one another, the boundary may be a diffuse one. More generally it may fluctuate to and fro with time and a tactical retreat in some areas of instrumentation may even be necessary to facilitate advances in others. The fog may lift to reveal new things (including corrections to current thinking) or we may rediscover previously known things or ideas that had been forgotten. None of this necessarily implies that the individual electron microscopist may not experience what has been termed a “single image epiphany” [4] or, when more prior thought is involved, their “eureka moment”. The more common result following the development of improved instrumentation is however a more nuanced blend of incremental progress with occasional surprises ranging from the half expected to potentially more revolutionary.

We illustrate these points with reference to the developments following aberration correction in Section 2 and for valence loss spectroscopy in Section 3. As discussed in Section 4, these earlier episodes may illuminate the still more complex “cutting edge” that is now unsheathed by the recent extension of electron spectroscopy towards 10 meV in the ultra-low loss region [3,5].

2. Aberration correction and projection imaging

Several comprehensive accounts provide different perspectives on the long saga culminating in the successful correction of lens aberrations in electron optics [6–8]. A particularly significant stage was passed when the resolution performance of an aberration corrected instrument surpassed that of any uncorrected microscope including high voltage microscopes [2,9]. Soon afterwards however it became apparent that some unexpected benefits were available beyond improved spatial resolution. In transmission electron microscopy (TEM) the useful imaging condition with a small negative spherical aberration was discovered [10] and more significantly in scanning transmission electron microscopy (STEM) a greatly increased probe current could be utilised [11].

In light element conductors, most notably graphene, the ability to get atomic resolution at beam voltages such as 60 keV below the threshold for knock-on damage was a further crucial and fruitful development. This area however also provides the first example to be noted here where an advance in TEM has brought us into more direct competition with another community namely scanning tunnelling microscopy (STM). We may have an advantage in being able definitely to identify specific atom species but it is not logical to dismiss STM work on graphene with the usual mantra that “it's just a surface technique”! Indeed it seems on balance more likely that eventual applications for graphene and similar single layer crystals will be found not in the free-standing form mostly used in TEM but as part of a supported structure of the kind usually studied by STM.

Of greater potential significance to the electron microscopy community itself is a still more recently emerging consequence of aberration correction – the development of depth sectioning techniques with the possible undermining of the projection imaging illusion which has been so pervasive in atomic column resolution in (S)TEM. In the early

<http://dx.doi.org/10.1016/j.ultramic.2016.11.006>

Received 16 September 2016; Received in revised form 4 November 2016; Accepted 15 November 2016

Available online xxxx

0304-3991/© 2016 Elsevier B.V. All rights reserved.

days of structure imaging, diffraction contrast experts expressed doubts over the feasibility of deriving valid 3-d structural information on this basis [12]. Even before that, Ondrej Krivanek's first research [13] on the structure of amorphous materials had made clear the shortcomings of the projection approximation in this extreme situation. Nevertheless it was he who swiftly moved on to produce the celebrated structural image of a grain boundary in Ge that provided early compelling evidence of what projection imaging could achieve in favourable cases [14]. All doubts were then swept away by the mighty tide of 2-d images obtained from beam-aligned interfaces. Many of the samples studied may indeed have a 2-d structure with a simple unit cell periodicity in the beam direction but in other cases we have to conclude that the effects of any more complex structure are usually suppressed in the image. From the many beautiful images of strontium titanate obtained in projection along a crystal axis for instance one would never realise that most of its surfaces reconstruct though they can reveal themselves in off-axis electron diffraction patterns [15] or in atomically resolved secondary electron emission [16]. Faceted nanoparticles often illustrate the same point in a single image since the side facets seen in projected profile view can partially reveal a reconstructed surface layer when any similar structure on the top and bottom surfaces is quite invisible in the image.

A great deal of structure imaging work has also been carried out for dislocations in cases where the dislocation line passes through the thin crystal in the direction of a prominent crystal axis which can be used as viewing direction. Interesting details of the structure in the dislocation core have thus been revealed in many different crystals. Again however the images do not seem to be sensitive to structural variations along the core that would arise from jogs or kinks. With the dislocation lying normal to the viewing direction i.e. in plan view, the highly kinked structure of a dissociated dislocation core was vividly demonstrated in a remarkable interference image using the zero order beam and the six nearest "forbidden" reflections in the first order Laue zone [17]. Sadly however this approach has not been repeated.

For images projected along a crystal axis, the origin of their insensitivity to more complex 3-d structural features is due to the electron channelling effect. Structural variations with a wavelength along the beam direction corresponding to an extinction distance would be picked up through transitions from one Bloch wave state to another but the channelling electron wave-field simply averages its way through more rapidly varying structures without obvious scattering and adapts adiabatically to more slowly varying structures [18]. In principle it might be possible to detect these effects by measuring image intensities but this is still very rarely done in (S)TEM.

The channelling effect operates for fast electrons travelling only in directions fairly close to a prominent crystal axis and the greatly increased collection or illumination angles that are now available in aberration-corrected (S)TEM go well beyond the typical threshold angle for dechannelling effects to set in. Electron microscopists may therefore find that their high resolution images display more sensitivity to the presence of the 3-d structures which they have hitherto been able to ignore! With the larger scattering angles that can now contribute to the image, greater depth sensitivity (i.e. less depth of field) can also be expected though the extent to which this can be exploited for depth sectioning can be complicated by any residual channelling effect.

An important milestone in this slow return of "cutting edge" high resolution electron microscopy to 3-d imaging is provided by a recent structural image analysis of an extended dislocation in GaAs studied in plan view and depth sectioning with a Nion STEM [19]. It will be very interesting to discover to what extent this reversion to an earlier form of imaging develops not only for dislocations but for other 3-d defects. The scattering from the defect region is much less in plan view since it does not extend all the way through the specimen as it would for a dislocation or interface aligned with the viewing direction. To be detectable therefore it will be essential to remove as much as possible of the background scattering from electronic excitations and phonons

as well as from surface contamination or reconstruction. The background elastic signal from the more nearly perfect crystal regions above and below the defect will of course still be present but could if necessary also be reduced by reverting to diffraction contrast weak beam imaging or to the method already mentioned of structure imaging with forbidden reflections [17]. Very recently it has been demonstrated that ptychography can offer a route to phase contrast imaging in the STEM, powerfully complementing the high angle dark field image simultaneously available [20]. Furthermore, depth-sectioned information can be obtained simply by post-processing the 4-d ptychography data set. The ptychography method employed [21] requires however that the specimen scattering can be described by a simple transmission function at each entrance surface position – a condition that is most easily met in very thin samples and at high beam energies.

3. Spatially localised valence loss spectroscopy

3.1. Electron energy loss and light scattering

Progress in accessing and interpreting localised electron energy loss spectroscopy (EELS) data in the valence excitation region from say 0.2–30 eV exhibits several of the complex features of advancing research which were outlined in the introduction. There were some early successes in using plasmon EELS for nanoanalysis in alloys and near defects in the period 1965–75 but these proved less generally useful than the core loss spectroscopy which substantially replaced them. The development of STEM EELS however allowed a few physics laboratories to cling on and address the challenge of extending Fermi's classical theory of dielectric excitation [22] to the nanometre scale. Detailed e-beam characterisation of the dielectric response of small particles was for instance demonstrated [23] by working not only with the usual penetrating beam but also in aloof beam excitation mode with reduced ionisation damage. Around 2000 this work provided a foundation for the great explosion of interest in nanoplasmonics generated by improvements in electron energy resolution into the sub 3 eV region. A recent review [24] sketches this sinuous historical trajectory together with a full and up to date account of recent progress for a range of nanostructures. Some results demonstrating the partial connection between EELS and cathodoluminescence (CDL) are included with an outline of the increasing involvement of electron microscopists with the photonics community on which it seems important to expand on further here.

Historically of course the work of Gustav Mie [25], describing the scattering and extinction of light on small dielectric spheres, anticipates to some extent the discovery of surface plasmons by Rufus Ritchie [26]. However the fundamental difference between photon and electron interactions in such cases is not usually given the emphasis required if papers are to be read by both communities. Quantum mechanically the absorption of light in which one photon disappears to create a real excitation of the specimen is a first-order transition (Fig. 1). Unlike the electron, the photon transfers all its energy $\hbar\omega$ as well as its momentum $\hbar k$ in the transition. It occurs only for frequencies in near resonance with the excitation and the event probability depends on the imaginary part ϵ_2 of the dielectric function. Away from resonance we can get photon scattering involving second-order processes (Fig. 1) with the absorption of one photon (ω, k) and the emission of another (ω', k') where the sample jumps from its initial state to a final state making use of a virtual intermediate state. This includes elastic scattering $\omega = \omega'$ when the sample is left in its initial state and the momentum transfer is related to its shape. Inelastic (Raman) scattering can also occur with for instance the creation or annihilation of a phonon. Other examples of the second-order Raman scattering process that can be observed with X-rays are Compton scattering and even real plasmon creation [27].

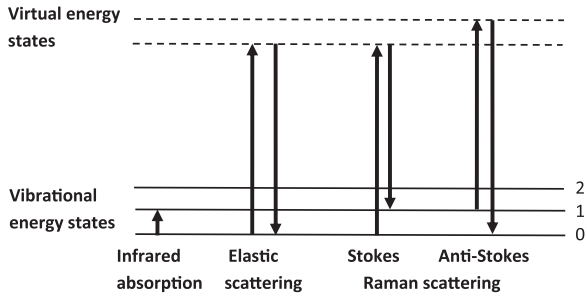


Fig. 1. Quantum mechanical optical transitions. Apart from absorption, the other scattering processes are second order involving an intermediate transition to a virtual state. In elastic scattering the object returns to its initial state (usually the ground state 0). In Stokes Raman scattering it returns to a state where a phonon has been excited. In anti-Stokes Raman scattering the specimen starts in an already excited state and returns to the ground state delivering energy to the light.

3.2. Principles of photo-induced near-field electron microscopy (PINEM)

In recent years the new and intriguing PINEM technique has been pioneered by the late Ahmed Zewail and co-workers [28,29]. Here, in a pump-probe arrangement, a specimen such as a carbon nanotube is subjected to a train of femtosecond laser pulses with photon energy $\hbar\omega$. Each pulse signal is also used to trigger the release from the electron gun of a few electrons to pass through the electron microscope column. When these electrons pass through the scattered photon near-field region close to the specimen where, in contrast to more familiar far-field plane wave region, exchange of energy and momentum with the light field is allowed [30], multiple energy losses and gains in units of $\hbar\omega$ are observed and have been theoretically analysed [30–33]. No energy in units of $\hbar\omega$ is transferred to or from the specimen since the light wave frequency ω is far from any resonance and its scattering is elastic. In principle some energy at surface plasmon or other frequencies characteristic of the specimen could be transferred to it from the electron in the usual aloof beam energy loss process or by Raman scattering of the light if it had sufficient energy but the probability of these is very low in comparison. Nevertheless these experiments throw up several novel questions for discussion.

Using those beam electrons which have experienced energy losses or gains $\hbar\omega$, the optical near-field close to a possibly complex nanostructure can be mapped often with spatial resolution better than could be achieved in near-field optical imaging and without the disturbing influence of a nano-tip. The mapping can also deal with so-called dark mode cases where the scattered light cannot escape to be detected in the usual far-field optical measurements. Although, as already noted, the quantum mechanical excitations of the sample are virtual rather than real, it is often easier to think classically that the elastically scattered optical field is generated by surface charges oscillating at the driving frequency ω [33,34]. This is after all the picture underlying the elastic scattering that yields X-ray diffraction patterns. In optical scattering, the spatial configuration of this oscillating charge is made up by virtually excited surface plasmons or other modes contributing amplitudes that depend on how near resonance they are as is indicated by recent observations on an Ag nanowire [35].

It has been suggested that we could learn even more about the sample by generating real excitations possibly by employing much less intense continuous PINEM illumination which could be tuned through the resonant frequencies [36]. In favourable cases, it might be possible with this optical stimulus to generate measureable electron energy loss and gain signals from excitations that would otherwise be too weak to detect [37]. Private communications from A. Zewail and G. Botton however warn that the specimen could often evaporate in such experiments! Suppose for instance that the dipolar surface plasmon on a 2 nm diameter spherical particle of Ag could be continuously boosted to the first excited state $\hbar\omega_s=3$ eV with a life time of 10^{-14} sec.

This corresponds to a power transfer of $P=5\times 10^{-5}$ W half of this which might be radiated directly by the dipolar surface plasmon and half going into electronic excitation leading to Stefan's law thermal radiation. With $\sigma AT^4=2.5\times 10^{-5}$ W and a particle area $A=4\pi\times 10^{-18}$ m² we get $T=7.5\times 10^4$ K! Secondary electron emission or heat loss by conduction to the substrate would reduce this but continuous laser boosting of such plasmons seems impossible. Resonant external boosting of excitations might still be feasible however at much lower frequencies in pump-probe schemes or, with chopped excitation and coincident chopping of the detection system and was indeed demonstrated many years ago at RF frequencies and below [38,39]. Very recently in pump-probe observations at THz frequencies the deflection, rather than the energy loss or gain, of a fast electron beam passing through a split-ring resonator has been demonstrated [40]. It should also be mentioned that more generally in pump-probe electron microscopy, real excitations of the specimen generated by the pump laser have been probed by penetrating rather than by aloof electron beams and often detected through subsequent secondary effects [29].

3.3. Electromagnetic potentials and the Schrodinger equation

In the presence of an electromagnetic (EM) field described by a vector potential $\mathbf{A}(\mathbf{r},t)$ and a scalar potential $\phi(\mathbf{r},t)$, the Schrodinger equation takes the form [41]

$$i\hbar\frac{\partial\psi}{\partial t}=\left[-\frac{\hbar^2}{2m}\nabla^2+\frac{ie\hbar}{mc}\mathbf{A}\cdot\nabla+\frac{ie\hbar}{2mc}(\nabla\cdot\mathbf{A})+\frac{e^2}{2mc^2}\mathbf{A}^2+e\phi\right]\psi \quad (1)$$

In not too strong fields the non-linear term in \mathbf{A}^2 , giving rise to ponderomotive forces and the Kapitza-Dirac effect, can be neglected. For a fast electron propagating with velocity $v=\hbar k/m$ close to the z direction we can further replace $(ie\hbar/mc)\mathbf{A}\cdot\nabla\psi$ with $-(ev/c)A_z\psi$. Most quantum mechanics textbooks then urge use of the Coulomb gauge \mathbf{A}^C,ϕ^C because $\nabla\cdot\mathbf{A}^C=0$ but ϕ^C has the unphysical property of propagation at infinite speed and, possibly as a consequence, \mathbf{A}^C is often difficult to calculate. If however we use the more familiar Lorentz gauge \mathbf{A}^L,ϕ^L where $\nabla\cdot\mathbf{A}^L=-c^{-1}\partial\phi^L/\partial t$, we may note that, when a simple frequency dependence $\exp[i\omega t]$ occurs, the term $(ie\hbar/2mc)\nabla\cdot\mathbf{A}^L=(\hbar\omega/2mc^2)e\phi^L$ and is therefore a negligible correction at optical frequencies.

An even simpler connection to the EM fields emerges [33] by noting that, when the incident fast electron is described by a wave function $\exp[i(kz-\Omega t)]$, exchange of energy is driven by the Fourier component $\exp[\pm i(\omega t-\omega z/v)]$ of the scattering potential $V(\mathbf{r},t)=-(ev/c)A_z(\mathbf{r},t)+e\phi(\mathbf{r},t)$. Here the upper sign refers to electron energy loss and photon energy gain. A particularly simple form for this Fourier component then becomes apparent.

$$e\left\{-\frac{v}{c}A_z(x,y)+\phi(x,y)\right\}\exp\left[\pm i\left(\omega t-\frac{\omega}{v}z\right)\right]=\pm\frac{v}{i\omega}eE_z(x,y)\exp\left[\pm i\left(\omega t-\frac{\omega}{v}z\right)\right] \quad (2)$$

This shows that the electric field component $E_z(\mathbf{r},t)=-c^{-1}\partial A_z/\partial t-\partial\phi/\partial z$ can be used directly to construct the effective scattering potential for all the inelastic scattering events. Earlier theories of PINEM [29–32] incorrectly assumed that the scalar potential vanished but nevertheless correctly used E_z in the final expression for the scattering.

Provided that $E_z(x,y)$ does not vary too rapidly, the inelastically scattered electron wave can then be described by an eikonal function as found previously [30–33].

$$\psi(\mathbf{r}, t) = \exp \left[i(kz - \Omega t) + i|I(\mathbf{r})| \cos \left(\frac{\omega z}{v} - \omega t + \delta \right) \right] = \exp \left[i(kz - \Omega t) \right] \left\{ J_0(|I(\mathbf{r})|) + 2 \sum_{n=1}^{\infty} i^n J_n(|I(\mathbf{r})|) \cos \left(\frac{n\omega z}{v} - n\omega t + nC \right) \right\} \quad (3)$$

where

$$|I(\mathbf{r})| \exp[i\delta(x, y)] = \frac{2e}{i\hbar\omega} \int_{-\infty}^z E_z(x, y, z') \exp \left[\frac{i\omega z'}{v} \right] dz' \quad (4)$$

The different terms in the curled brackets in Eq. (3) correspond to the zero loss amplitude and to the various energy gain and loss peaks in multiples of $\hbar\omega$. In the approach used here, not involving creation and annihilation operators for the photon states, the energy loss and gain probabilities are equal. The theory appears to work quantitatively when compared in detail with observations even in some cases with multiple losses extending as far as $n=40$ [31]. The validity of neglecting the A^2 term in Eq. (1) in such extreme circumstances needs to be checked however. Eq. (3) also displays in its downstream propagation the formation of extremely sharp pulses [42] but, since they may well contain only one electron, it is not yet clear what the practical significance may be.

Some information about the angular deflections and consequent spreading of the electron beam in the x and y directions is also suggested by Eqs. (3) and (4). These deflections originate in the x, y dependence of E_z and could therefore through Maxwell's equations be associated with magnetic field components B_y and B_x . This may be a little puzzling since in aloof beam scattering the transverse force from the induced field electric component E_x also plays a strong role [43]. It would undoubtedly be more realistic to study these processes with a focused incident probe function than with a plane wave but it would then be necessary to investigate more carefully the validity of not only the eikonal solution but also of some of the approximations made with Eq. (1). One might conjecture that, for the usual symmetrical probe, the terms discarded in Eq. (1) involving x and y derivatives would cancel and that any failure of the eikonal approximation would be governed mainly by lateral spreading due to probe dispersion but these ideas could obviously be checked by numerical integration. As discussed in the next section, such studies with an incident probe would also be important in exploring the application of the PINEM theory to deal with more typical aloof beam STEM experiments in the absence of laser illumination.

3.4. Spontaneous near-field theory of fast electron inelastic scattering

In PINEM the fast electron experiences possibly multiple interactions with the near-field region of the optical EM field through which it passes. Even in the absence of any externally imposed EM field however, the electron will still pass through the fields generated by the excitations of the specimen itself either in their zero point mode or some thermally excited higher mode and these fields could, as in the PINEM interaction, deliver to the electron energy losses or gains at the relevant specimen excitation frequency [37]. This spontaneous near-field mechanism is radically different than the generally used Fermi theory [22] of dielectric excitation by a fast electron where the electric field that acts classically to produce a retarding force on the electron is regarded as having been induced by the electron's self field carried with it in its passage through or near the dielectric. In computing thermal diffuse scattering, rather than thinking of the phonon response induced by the fast electron, it is indeed the spontaneous phonon potential field approach that is universally used albeit sometimes in the frozen phonon approximation. Quantitative comparison of the two approaches for dielectric excitations in simple structures would be useful in deciding whether the spontaneous near-field mechanism is an alternative to the Fermi method or represents some kind of additional

contribution. In both theories the primary interaction is through the z component of the electric field E_z . Three other interesting points of comparison between the two theories can be identified.

For a fast ion of charge Ze , the Fermi theory gives an induced field E_z proportional to Z which, acting on a charge Ze , results in a retarding force proportional to Z^2 . In this classical theory the loss probability and stopping power therefore also behave like Z^2 . The spontaneous field is however independent of Z and thus, acting on the charge Ze , gives a potential proportional to Z . This potential however has to be treated quantum mechanically not classically and in first Born (single scattering) approximation gives a loss probability also proportional to Z^2 .

Irrespective of the quantal nature of the solid state excitation – boson (e.g. plasmon or phonon) or fermion (e.g. two level system), the associated spontaneous oscillatory fields in and near the solid are all EM boson modes of a cavity. In the excited state when interacting with a fast electron these spontaneous fields therefore give the usual boson energy loss and gain probabilities consistent with the fluctuation-dissipation theorem. In the Fermi excitation model, the same balance of energy loss and gain probabilities would apply where the electron interacts directly with a solid state boson excitation such as a plasmon but the situation is less clear when the interaction is with a fermion excitation.

It has already been noted [37] that these spontaneously fluctuating fields can have different symmetries than those excited by a fast electron on a classical trajectory. In situations of high resolution imaging or electron holography where a wave description of the fast electron is essential, scattering from these fields of different symmetry could then produce additional electron beam incoherence.

4. Spatially localised EELS in the thermal excitation region

4.1. Finding our place at low frequencies

The development of a monochromated STEM system [3] offering energy resolution in EELS approaching 10 meV may yield sharper spectra in the already well exploited core and valence excitation regions but more importantly opens up quite new fields for electron microscopy at ultra-low energy excitations. Significant phenomena in this region such as molecular bond vibrations, optical phonons, polaritons, infrared (IR) excitations, carrier plasmons in semiconductors etc have however all been subject to intense study for many years. The classical broad beam techniques extensively used supply spectral data averaged over the whole specimen, a relevant example here being the coupling between carrier plasmons and optical phonons investigated through EELS with 5 eV electrons and 10 meV energy resolution [44]. Sometimes these broad beam spectra contain contributions ascribed to concentrations of defects or other specific sites. Occasionally, for example in the terahertz excitation of complex nanostructures, numerical simulation may then bridge the vast gulf to identify the precise defect or other structural feature involved [45]. Broad beam methods have also been used to address surface problems notably in the study of polaritons and other surface excitations by EELS in transmission by Boersch et al. with 25 keV electrons in transmission [46] and by Ibach et al. using low energy reflection EELS [47].

More recently however, spatially localised information has been acquired on the scale of a 20 nm tip by near-field optical microscopy (NFOM) for optical modes in a BN nanotube [48] and for specific surface sites using IR absorption [49] or Raman scattering [50]. With much higher atomic resolution, inelastic tunnelling spectroscopy in STM has been used to image the 358 meV bond vibration in an isolated acetylene molecule on the surface of Cu [51]. These NFOM and STM methods can even be applied in radiation-sensitive samples where TEM investigations could cause difficulties. The challenge is therefore to identify important problems where the imaging capability or other advantages conveyed by electron microscopy could now make a

difference.

4.2. Ultra-low energy loss aloof beam STEM EELS

Using ultra-low energy STEM EELS, there has recently been encouraging success in detecting firstly an optical vibrational mode at 138 meV in SiO₂ [3] and more recently in the 200–400 meV range the C=O, C–H and N–H bond stretching modes in a guanine crystal [5]. This work was mostly done in aloof beam mode at rather large impact distances b

>20 nm from the crystal surface thus greatly reducing the ionisation damage generally triggered by higher losses that can be excited only at smaller impact distances [23,52]. The inverse relation between impact distance b and energy transfer $\hbar\omega$ is embedded in the characteristic parameter $\xi=\omega b/v$ governing the non-relativistic loss probability in EELS. For an aloof beam trajectory of length L at distance b from the planar surface of a material with dielectric response function $\varepsilon(\omega)$ the loss probability $P(\omega)$ per unit energy range is given in atomic units by the expression [53].

$$P(\omega)=\left[\frac{2L}{\pi v^2}\right]K_0\left(\frac{2\omega b}{v}\right)Im\left\{-\frac{2}{\varepsilon(\omega)+1}\right\} \quad (5)$$

The linear dependence of $P(\omega)$ on the modified Bessel function $K_0(2\xi)$ was shown to give a good description of these latest results with typical values of $v/2\omega=250$ nm [3,5]. At large distances the K_0 function falls off as $\exp[-2\xi]/\sqrt{\xi}$ but, on progressing to smaller distances $\xi\ll 1$, it rises much more steeply due to increasing contributions from higher momentum components of the surface response. Working at smaller values of b therefore yields not only a stronger signal but also better spatial resolution (in projection) of any surface structure. In guanine, because of increasing ionisation damage at small b values, it was not possible to work below $b=20$ nm so spatial resolution of about that amount might be expected provided that there is enough signal. This modest resolution could still be useful in electron microscopy as an aloof beam, damage-free source of in-situ infrared absorption data but better imaging performance would obviously be very desirable.

To detect a bond stretching mode for a single molecule isolated on a surface by aloof beam spectroscopy will certainly be very much harder than detecting the signal from a whole crystalline assembly of such molecules as in the guanine example. Again in atomic units, the dipole loss probability $P(\omega)$ per unit energy range for an aloof beam passing at distance b from the centre of a small dielectric sphere of radius a is given by the expression [53]

$$P(\omega)=\left[\frac{4a}{\pi v^2}\left(\frac{\omega a}{v}\right)^2\right]K_n^2\left(\frac{\omega b}{v}\right)Im\left\{\frac{\varepsilon-1}{\varepsilon+2}\right\} \quad (6)$$

where $n=0$ for a dipole aligned with the e-beam and $n=1$ for a dipole normal both to the surface and to the beam trajectory. A molecule with a dipole vibration mode at 200 meV may be regarded as equivalent to a polarisable sphere with $a=0.1$ nm and $a\omega/v=2\times 10^{-4}$. Assuming $a/L=10^{-2}$, the quantity in square brackets in Eq. (6) is less than the one in Eq. (5) by a factor of 4×10^{-10} . Although the Bessel function K_1^2 in Eq. (6) compared with K_0 in Eq. (5) might provide a compensating factor of about 10^6 at very small impact distances $b=0.5$ nm, the signal will clearly be very weak. To provide some depth resolution as well as lateral resolution, it might then be advantageous to operate in glancing angle reflection electron microscopy (REM) mode rather than with the parallel aloof beam trajectory (Fig. 2). This mode could also reduce both the background signal from other parts of the surface as well as radiation damage. As discussed in the next section, a more localised and possibly even larger signal than that from the oscillating dipole might then be available from impact scattering with the vibrating atoms [47,54].

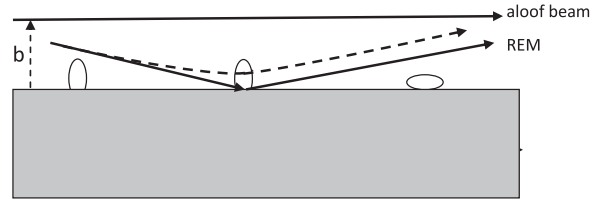


Fig. 2. Aloof beam and REM sampling of vibrating molecules at a surface. Under negative charging of the specimen, a still more useful trajectory indicated by the broken line might be followed.

4.3. Ultra-low energy loss STEM EELS with penetrating beam electrons

The differential cross section for the scattering of an electron by a vibrating diatomic molecule with the usual reduced mass $\mu=m_1m_2/(m_1+m_2)$ can be described with an extended form of an expression recently given by Rez [55] using the spontaneous near-field theory discussed above.

$$\frac{d\sigma}{d\Omega}=\left|iq\cdot\mathbf{u}\left\{\frac{\mu}{m_1}\left[\frac{\Delta Q}{a_0q^2}+f_1^n(q)\right]e^{-iq\cdot\mathbf{R}}+\frac{\mu}{m_2}\left[\frac{\Delta Q}{a_0q^2}-f_2^n(q)\right]e^{iq\cdot\mathbf{R}}\right\}\right|^2 \quad (7)$$

For simplicity here the electron scattering factor f^n for each atom in the neutral state is supplemented with an additional Coulomb scattering term from a charge $+\Delta Q$ or $-\Delta Q$ placed at each atomic centre. The displacements of the ions from their equilibrium positions at $\pm\mathbf{R}$ in the x,y plane are $\mathbf{u}_1=\mu\mathbf{u}/m_1$ and $\mathbf{u}_2=-\mu\mathbf{u}/m_2$ and are along the bond direction \mathbf{R} . Rez [55] did not present the detailed dependence on scattering vector $\mathbf{q}=(q_x, q_y, \omega/v)$ shown in Eq. (7). He decided to neglect the impact scattering terms in f^n but concluded that typical cross sections could nevertheless be similar to those for inner shell excitations if scattering angles up to 100mrad could be collected.

The two ionic dipole oscillators, which have opposite charges ΔQ as well as displacements, scatter in phase at small values of q . They are characterised for similar masses by $2\cos(\mathbf{q}\cdot\mathbf{R})/q^2$, and dominate the scattering giving rise to the nanometre-range near-field effects already considered. In this low q region the impact scattering from the neutral atom terms is small, particularly if the two atoms have fairly similar mass. At somewhat larger values of $q > R^{-1}$, impact scattering dominates and may therefore make a significant contribution to the overall signal for modest scattering angles within the range considered by Rez. The dependence of the scattering on $\mathbf{q}\cdot\mathbf{u}f(q)$, familiar in STEM diffuse scattering and typically peaking at an angle greater than spectrometer apertures or even most probe forming apertures, is complicated here by interference oscillations between the two atomic contributions. Since at moderate electron scattering angles f^n increases sub-linearly as a function of m , the lighter of the two atoms will make the larger contribution. The full impact scattering is evidently most directly selected at very small (atomic-scale) impact parameters and at fairly large scattering angles, possibly using an off-axis detector.

The additional features of ultra-low loss electron scattering which arise inside a crystal can be illustrated by reference to the scattering potential generated by a phonon. For a crystal whose unit cell contains neutral atoms with scattering factors $f_j(q)$ at mean positions $\boldsymbol{\rho}_j$ the first order impact scattering due each atom's displacement $\mathbf{u}_j\exp[i\mathbf{q}\cdot\mathbf{r}-i\omega t]$ in a phonon vibration mode (with a wave vector \mathbf{q} confined to the first Brillouin zone) is described by a potential

$$V(\mathbf{r}, t)=i\Sigma_{\mathbf{g}}\exp[i(\mathbf{q}+\mathbf{g})\cdot\mathbf{r}-i\omega t]\{\Sigma_j(\mathbf{q}+\mathbf{g})\cdot\mathbf{u}_j f_j(\mathbf{g})\exp[i\mathbf{g}\cdot\boldsymbol{\rho}_j]\} \quad (8)$$

If some of the atoms are ionised, an extra small-angle scattering contribution similar to that already employed in Eq. (7) would arise in the $\mathbf{g}=0$ term. The polariton excitations which then arise from the coupling between these optically active phonons and photons are well understood [56] in conjunction with a dielectric formalism convenient for fast electron excitation [57]. They have recently been successfully

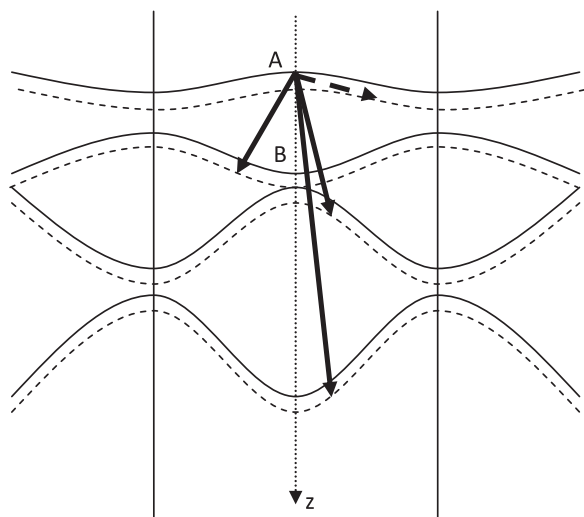


Fig. 3. Bloch wave dispersion bands for a fast electron of energy E (solid lines) and an electron of energy $E' = E - \hbar\omega$ (broken lines). The latter are displaced to smaller values of k_z by a distance ω/v which for phonon excitation would be invisibly small in the figure. From a starting state A, inelastic transitions due to phonon excitation can be intra-band (broken arrow) or, with much larger longitudinal momentum change q_z , inter-band transitions (solid arrows).

detected by STEM in aloof beam as well as in penetrating beam mode [3]. In aloof beam mode the observed long range dependence on impact parameter appears to be consistent with the ionic ($\mathbf{g}=0$) term and near-field theory. A much more rapid variation of the loss signal with impact parameter was noted however with a penetrating beam passing near and parallel to a boundary between Si and SiO₂ and this may possibly be due to impact (i.e. umklapp) scattering from the $\mathbf{g}\neq 0$ terms in Eq. (8).

As it stands Eq. (8) should be adequate for describing phonon excitation in metals where any dose limitations due to ionisation damage can be ignored. The term in curled brackets describes in diffraction space the scattering in the vicinity of each Bragg reflection \mathbf{g} with the largest contribution coming from moderately large values of g . In thin crystals the single phonon scattering approximation of Eq. (8) may still be reasonably valid though the scattering transitions will be between Bloch wave states rather than between plane wave states (see Fig. 3). It is then interesting to note that the $\mathbf{g}=0$ term drives mainly intra-band inelastic transitions requiring as before $q_z = \omega/v$ whereas the $\mathbf{g}\neq 0$ terms drive inter-band transitions $i \rightarrow j$ requiring a larger longitudinal momentum change $q_z = \omega/v + \Delta k_{ij}$. The strongest transitions will be to Bloch wave states with large contributions from high g components and only small contributions from small g components and could thus involve values of q_z large enough to invalidate any projection approximation in imaging. It also follows that, unless multiple phonon scattering is significant, Bragg reflections in the perfect crystal will probably not bring the strong phonon scattering intensities back close to the axis.

It will be a very challenging task to build a high quality spectrometer working out to the rather large angles where the phonon scattering peaks although some encouraging progress in this direction has been reported [58]. It could be easier to retain the current spectrometer design in conjunction with large angle hollow-cone illumination. In view of the likely failure of the projection approximation, an even better option in the author's opinion would be to revert to diffraction contrast dark field imaging selecting the diffuse scattering in the vicinity of a specific Bragg spot \mathbf{g} as is indicated in Fig. 4. This method would also reveal more directly perhaps than structure imaging the phonon polarisation and displacements within the unit cell. It would again require tilted illumination but with a less tightly focused spot since the spatial resolution would not be below unit cell level.

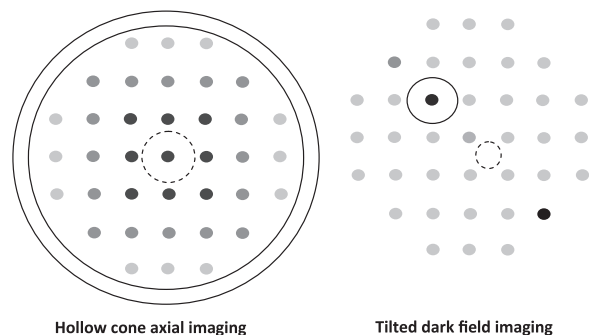


Fig. 4. Probe forming apertures and spectrometer collection apertures are shown in full and broken lines respectively for axial and dark field diffraction contrast imaging. In the latter case both the crystal and the illumination are tilted to excite the high-order Bragg reflection shown with the spectrometer collecting diffuse scattering on axis.

It seems unlikely that electron microscopy can now add anything of significance to the investigation of phonons in perfect crystals. Phonons localised at internal interfaces or at line or point defects however provide a field which is largely unexplored experimentally. The average effect of point defect concentrations on phonon spectra can be detected by broad beam methods. The results [59] support the early theory [60] that identifies resonance states within the phonon bands caused by heavy impurities and for light impurities more localised phonon states occurring at the zone boundary in the gap between bands or above the highest band. For a Cu 4% Al alloy, the Al atoms were shown to generate a localised mode near the (111) Brillouin zone boundary lying at 9 THz (i.e. 36 meV) and thus slightly above the maximum band frequency of 7 THz at this point [59].

The single phonon scattering assumption made so far may fail; firstly because in a thick enough crystal the fast electron may make more than one phonon collision and secondly because, even in a single collision, the momentum transfer may be great enough to drive the phonon excitation into the anharmonic region. The latter situation is more likely when the electron collision is effectively with a single atom rather than with several neighbouring atoms in a column. The possibility has been discussed [37] of studying as a function of increasing momentum transfer the transition from phonon excitation to single atom recoil and even knock-on damage. In this context it would be particularly interesting to discover whether there is some intermediate range of momentum transfer sufficient to define a recoil energy characteristic of the struck atom rather than of the phonon but accessible at beam energies below the threshold for knock-on damage. Localised atomic mass spectroscopy, already shown to be feasible [58] would then be possible in a damage-free mode.

5. Conclusions

Although the development of electron microscopy instrumentation and technique will no doubt continue to present interesting challenges to its dedicated practitioners, the need to understand and respond to the activities of related research communities is pressing. As recounted here this problem has already become apparent in the surge of activity in plasmonics. In developing useful applications of ultra-low EELS, close cooperation with an even wider range of colleagues including scanned probe microscopists, IR spectroscopists, terahertz engineers etc. will be necessary. The novel contributions that the electron microscopist can bring to the party will be crucial. Spatial resolution may be the most obvious but as noted above aberration correction may not be necessary. Adequate and indeed more informative spatial information could be acquired if diffraction contrast imaging were more readily available, particularly in conjunction with tilted or hollow cone illumination to define a larger momentum transfer. Just as this paper was about to be submitted, Christian Dwyer kindly provided information on recent success in imaging polariton modes in BN with a

spatial resolution of about 1 nm [61]. This achievement depended on using off-axis detection of the diffuse scattering between the lowest order Bragg spots and might be able to yield even higher spatial resolution and even stronger signal by going to larger scattering angles indicated for example in Fig. 4.

In the absence of an aberration corrector, it could well be important to devote resources and space in the EM column to incorporating facilities such a secondary electron (SE) and CDL detection. Adding coincidence detection for CDL and EELS would for example usefully distinguish the part of the CDL signal arising directly from radiative decay of e-beam excitations like surface plasmons and the part arising from secondary decays after a cascade of energy transfers.

With care taken to limit excessive energy and momentum transfer it may be possible to carry out both vibration spectroscopy and atomic mass spectroscopy with zero or minimal ionisation or knock-on damage. Resonant stimulation of the sample with continuous optical radiation may be too damaging but could perhaps be carried out in pump-probe or chopped mode with phase sensitive detection of e-beam deflections. These procedures would be easier at lower frequencies and so give the possibility of spectral probing far below any limit set by electron spectroscopy.

Acknowledgements

I am grateful to Christian Dwyer, Sang Tae Park, Gianluigi Boton, Peter Crozier, Peter Rez, and to the late Ahmed Zewail for helpful discussions.

References

- [1] O.L. Krivanek, C.C. Ahn, R.B. Keeney, Parallel detection electron spectrometer using quadrupole lenses, *Ultramicroscopy* 22 (1987) 103–115.
- [2] P.E. Batson, N. Delby, O.L. Krivanek, Sub-angstrom resolution using aberration corrected electron optics, *Nature* 418 (2002) 617–620.
- [3] O.L. Krivanek, T.C. Lovejoy, N. Delby, et al., Vibrational spectroscopy in the electron microscope, *Nature* 514 (2014) 209.
- [4] A. Howie, Learning from past epiphanies, successes and disappointments to anticipate progress in electron microscopy, *Microsc. Microanal.* 18 (S2) (2012) 1948–1949.
- [5] P. Rez, T. Aoki, K. March, et al., Damage-free vibrational spectroscopy in the electron microscope, *Nat. Commun.* 7 (2016) 11592.
- [6] H. Rose, History of direct aberration correction, *Adv. Imaging Electron Phys.* 153 (2008) 1–37.
- [7] P.W. Hawkes, Aberration correction past and present, *Philos. Trans. Roy. Soc. A367* (2009) 3637–3664.
- [8] O.L. Krivanek, N. Dellby, M.F. Murfitt, Aberration correction in electron microscopy, in: J. Orloff (Ed.) *Handbook of Charged Particle Optics*, CRC Press, Boca Raton, FL, 2008, pp. 601–640.
- [9] P.D. Nellist, M.F. Chisholm, N. Dellby, O.L. Krivanek, et al., Direct sub-angstrom imaging of a crystal lattice, *Science* 305 (2004) 1741–1742.
- [10] C.J. Jia, L. Houben, A. Thust, et al., On the benefit of the negative-spherical-aberration –imaging for quantitative TEM, *Ultramicroscopy* 110 (2010) 500–505.
- [11] D.A. Muller, L. Fitting Kourkoutis, M. Murfitt, et al., Atomic-scale chemical imaging of composition and bonding by aberration-corrected microscopy, *Science* 319 (2008) 1073–1076.
- [12] G.R. Antis, D.J.H. Cockayne, Calculation and interpretation of high-resolution electron-microscope images of lattice defects, *Acta Cryst. A* 35 (1979) 511–524.
- [13] O.L. Krivanek, P.H. Gaskell, A. Howie, Seeing order in amorphous materials, *Nature* 262 (1976) 454–457.
- [14] O.L. Krivanek, S. Isoda, K. Kobayashi, Lattice imaging of a grain boundary in crystalline germanium, *Philos. Mag.* 36 (1977) 931–940.
- [15] A. Subramanian, L.D. Marks, Surface crystallography in the electron microscope, *Ultramicroscopy* 98 (2004) 151–157.
- [16] J. Ciston, H.G. Brown, A.J. Alfonso, et al., Surface determination through atomically resolved secondary-electron imaging, *Nat. Comm.* 6 (2015) 7358.
- [17] H.R. Kolar, J.C.H. Spence, H. Alexander, Observation of moving dislocation kinks and unpinning, *Phys. Rev. Lett.* 77 (1996) 4031–4034.
- [18] P.B. Hirsch, A. Howie, R.B. Nicholson, et al., *Electron Microscopy of Thin Crystals*, Krieger, New York, 1977.
- [19] H. Yang, J.G. Lozano, T.J. Pennycook, et al., Imaging screw dislocations at atomic resolution by aberration-corrected electron optical sectioning, *Nat. Comm.* 6 (2015) 7266.
- [20] H. Yang, R.N. Rutte, L. Jones, et al., Simultaneous atomic-resolution electron ptychography and Z-contrast imaging of light and heavy elements in complex nanostructures, *Nat. Comm.* 7 (2016) 12532.
- [21] J. Rodenburg, R.H.T. Bates, The theory of super-resolution electron microscopy via Wigner-distribution deconvolution, *Philos. Trans. Roy. Soc. A* 339 (1992) 521–553.
- [22] E. Fermi, The ionization loss of energy in gases and condensed materials, *Phys. Rev.* 57 (1940) 485–493.
- [23] M.G. Walls, A. Howie, Dielectric theory of localised electron energy loss spectroscopy, *Ultramicroscopy* 28 (1989) 40–42.
- [24] C. Colliex, M. Kociak, O. Stephan, Electron energy loss spectroscopy imaging of surface plasmons at the nanometer scale, *Ultramicroscopy* 162 (2016) A1–A24.
- [25] G. Mie, Articles on the optical characteristics of turbid tubes, especially colloidal metal solutions, *Ann. Phys.* 25 (1908) 377–445.
- [26] R.H. Ritchie, Plasma losses by fast electrons in thin films, *Phys. Rev.* 166 (1957) 874–881.
- [27] P. Caduzzo, K.O. Routsalainen, C.J. Sahle, et al., High-energy collective electronic excitations in layered transition-metal dichalcogenides, *Phys. Rev. B* 90 (2014) 125125.
- [28] B. Barwick, D.J. Flannigan, A.H. Zewail, Photon-induced near-field electron microscopy, *Nature* 462 (2009) 902–906.
- [29] D. Shorokhov, A.H. Zewail, Perspective: 4D ultrafast electron microscopy-evolutions and revolutions, *J. Chem. Phys.* 144 (2016) 080901.
- [30] F.J. Garcia de Abajo, M. Kociak, Electron energy-gain spectroscopy, *New J. Phys.* 10 (2008) 073035.
- [31] S.T. Park, M. Lin, A.H. Zewail, Photon-induced near-field electron microscopy (PINEM): theoretical and experimental, *New J. Phys.* 12 (2010) 33502.
- [32] A. Howie, Photon interactions for electron microscopy interactions, *Eur. Phys. J. Appl. Phys.* 54 (2011) 33502.
- [33] S.T. Park, A.H. Zewail, Photon-induced near-field electron microscopy: mathematical formulation of the relation between experimental observables and the optically driven charge density of nanoparticles, *Phys. Rev. A* 89 (2014) 013851.
- [34] F.J. Garcia de Abajo, B. Barwick, F. Carbone, Electron diffraction from plasmon waves, *Phys. Rev. B* 94 (2016) 041404(R).
- [35] L. Piazza, T.T.A. Lummen, E. Quinonez, et al., Simultaneous observation of the quantization and the interference pattern of a plasmonic near field, *Nat. Comm.* 6 (2015) 6407.
- [36] A. Asenjo-Garcia, F.J. Garcia de Abajo, Plasmon energy gain spectroscopy, *New J. Phys.* 15 (2013) 103021.
- [37] A. Howie, Stimulated excitation electron microscopy and spectroscopy, *Ultramicroscopy* 151 (2015) 116–121.
- [38] P. Poncharal, Z.L. Wang, D. Ugarte, W.A. de Heer, Electrostatic deflections and electro-mechanical resonances of carbon nanotubes, *Science* 313 (1999) 1756–1759.
- [39] D.G. Davies, Scanning electron acoustic microscopy and its applications, *Philos. Trans. R. Soc.* 320 (1986) 243–255.
- [40] A. Ryabov, P. Baum, Electron microscopy of electromagnetic wave forms, *Science* 353 (2016) 374–377.
- [41] L.I. Schiff, *Quantum Mechanics*, McGraw-Hill, New York, 1949.
- [42] A. Feist, K.E. Echternkamp, J. Schauss, et al., Quantum coherent optical phase modulation in an ultrafast transmission electron microscope, *Nature* 521 (2015) 200–203.
- [43] A. Rivacoba, N. Zabala, Relativistic force between fast electrons and planar targets, *New J. Phys.* 16 (2015) 023012.
- [44] R. Matz, H. Luth, Conduction-band surface plasmons in the energy loss spectrum of GaAs (110), *Phys. Rev. Lett.* 46 (1981) 500–503.
- [45] P.Q. Liu, I.J. Luxmoore, S.A. Mikhailov, et al., Highly tunable hybrid metamaterials employing split-ring resonators strongly coupled to graphene surface plasmons, *Nat. Comm.* 6 (2015) 8969.
- [46] H. Boersch, J. Geiger, W. Stickel, Interaction of 25 keV electrons with lattice vibrations in LiF, *Phys. Rev. Lett.* 17 (1966) 379–382.
- [47] H. Ibach, D.L. Mills, *Electron Energy-loss Spectroscopy and Surface Vibrations*, Academic Press, Cambridge Mass. US, 1982.
- [48] L. Gilburd, X.G. Xu, Y. Bando, et al., Near-field infrared pump-probe imaging of surface phonon coupling in boron-nitride nanotubes, *J. Phys. Chem. Lett.* 7 (2016) 289–294.
- [49] F. Huth, A. Govyadinov, S. Amarie, et al., Nano-FTIR absorption spectroscopy of molecular fingerprints at 20 nm spatial resolution, *Nano Lett.* 12 (2012) 3973–3978.
- [50] S. Mignuzzi, N. Kumar Kumar, B. Brennan, et al., Probing individual point defects in graphene via near-field Raman scattering, *Nanoscale* 7 (2015) 19413–19418.
- [51] B.C. Stipe, Single molecule vibrational spectroscopy and microscopy, *Science* 280 (1998) 1732–1735.
- [52] R.F. Egerton, Vibration loss EELS and the avoidance of radiation damage, *Ultramicroscopy* 159 (2015) 95–100.
- [53] F.J. Garcia de Abajo, Optical excitations in electron microscopy, *Rev. Mod. Phys.* 82 (2010) 1–45.
- [54] C. Dwyer, Localization of high-energy electron scattering from atomic vibrations, *Phys. Rev. B* 89 (2014) 054103.
- [55] P. Rez, Is localised infrared spectroscopy now possible in the electron microscope?, *Microsc. Microanal.* 20 (2014) 671–677.
- [56] N.W. Ashcroft, N.D. Mermin, *Solid State Physics*, Rinehart and Winston, New York, 1976 (Chapters 26 and 27).
- [57] P.M. Echenique, A. Howie, Image force effects in electron microscopy, *Ultramicroscopy* 16 (1985) 269–272.
- [58] T.C. Lovejoy, N. Dellby, T. Aoki et al., Energy-filtered high-angle dark field mapping of ultra-light elements, in: *Microscopy and Microanalysis 2014 Conference Abstract*.
- [59] R.M. Nicklow, *Dynamic properties of defects*, in: J.N. Munday (Ed.), *Methods of Experimental Physics* 21, Academic Press, New York, 1983, pp. 172–193.
- [60] A.A. Maradudin, E.W. Montroll, G.H. Weiss, *Theory of lattice dynamics in the harmonic approximation*, in: F. Seitz, D. Turnbull (Eds.), *Solid State Physics Advances in Research and Applications*, Academic Press, New York, 1963 (Suppl. 3).
- [61] C. Dwyer, T. Aoki, P. Rez, et al., Electron beam mapping of vibrational modes with nanometer spatial resolution, *Phys. Rev. Lett.*, in press, 2016 submission .